Materials Today: Proceedings 65 (2022) 2138–2143

Contents lists available at ScienceDirect

Materials Today: Proceedings

journal homepage: www.elsevier.com/locate/matpr

Evaluation of the influence of alumina nano-particle size and weight composition on the corrosion resistance of monolithic AA1070 aluminium

Roland Tolulope Loto *, Philip Babalola

Department of Mechanical Engineering, Covenant University, Ogun State, Nigeria

ARTICLE INFO

Article history:
Available online 11 May 2022

Keywords:
Alumina
Corrosion
Composite
Aluminum

ABSTRACT

Corrosion resistance of AA1070 aluminium alloy (AA1070) was compared to AA1070 reinforced with alumina at weight composition (wt. %) of 5% and 10%, and grain size of 150 nm and 600 nm. Potentiodynamic polarization and open circuit potential analysis were employed in 0.0125 M H_2SO_4, 3.5% NaCl and 0.0125 M H_2SO_4-3.5% NaCl solutions. Data showed 0.0125 M H_2SO_4-3.5% NaCl solution was the most deleterious with peak corrosion rate value of 6.682 mm/y while 3.5% NaCl solution was the weakest with peak value of 0.084 mm/y. AA1070 at 5% (wt. %) and 150 nm particle size generally displayed the highest corrosion rate with values between 0.084 and 6.682 mm/y. However, visible decrease in corrosion rate occurred with increase in alumina weight fraction and particle size due to growth of the protective oxide on the composite and reduction of discontinuities to minimal values between 0.031 and 2.192 mm/y at 10% alumina weight fraction and 600 nm particle size. Cathodic and anodic reaction mechanisms significantly differs with respect to the electrolyte. Anodic reaction mechanism appeared under activation control in the sulphate-chloride and chloride solution, compared to cathodic reaction mechanism in the sulphate and sulphate-chloride solutions. Significant anodic degradation reaction was prevalent on the anodic polarization plot in the sulphate solution. Plots from open circuit potential analysis shows the composites and monolithic Al were the most thermodynamically stable in H_2SO_4 solution. In the sulphate-chloride solution, significant potential transients coupled with high corrosion tendency are conspicuous. The plot showed chaotic thermodynamic behaviour active passive transition behaviour of the passive film.

Selection and peer-review under responsibility of the scientific committee of the International Conference on Engineering for a Sustainable World.

1. Introduction

Appropriate materials selection is of utmost importance in the design of engineering parts, components and devices for industrial, civil and consumer applications to meet the requirements of astringent service conditions [1,2]. Light-weight materials which combine excellent strength with appreciable fatigue resistance and toughness are nearly impossible with monolithic metals. Secondly, operating environments (temperature, humidity, pressure, loading conditions etc.) tends to alter the properties of metals and alloys, hence reducing their functional lifespan [3]. Combining two or more materials together imparts properties otherwise absent in monolithic materials. Aluminium (Al) is the most copious metal on earth, making up about 8% of the earth's crust. Al alloy has extensive application in most industries due to its excellent mechanical properties and light weight [4]. However, in extreme conditions its versatility is limited. Aluminum metal matrix composites (AMMC) belongs to the category of light weight structural engineering materials which exhibits superior performance to monolithic aluminum. AMMC have wide-range application in the manufacture of automobile engine blocks, parts and components, biotechnology, consumer products, semiconductor in electronics, structural parts and components in aerospace, military applications, marine applications etc. [5]. Composites added to Al to improve its mechanical, structural and high temperature properties includes SiC, Al_2O_3, TiO, B_4C etc. through specialized industrial processes. These composites act as grain reinforcement within the

* Corresponding author.
E-mail address: tolulope.loto@gmail.com (R. Tolulope Loto).

https://doi.org/10.1016/j.matpr.2022.05.012
2214-7853/
Selection and peer-review under responsibility of the scientific committee of the International Conference on Engineering for a Sustainable World.

metallurgical structure of Al. The composites enhance the thermal conductivity of AMMC, resistance to abrasion, creep and stiffness coupled with good strength to weight ratio. Alumina is an Al oxide which occurs in nature as bauxite or corundum, and is an inert, thermally unstable, insoluble, amorphous and odorless material. It is used as a ceramic material, desiccating agent, prostheses, bionic implants, bullet proof armor, high-temperature furnace insulators etc. [6]. The high hardness value of alumina, its inert nature, high melting point and resistance to wear; accounts for its appreciable resistance to corrosion compared to other composite additions in Al [7–13]. The presence of composites exposes the AMMC to corrosion due to discontinuities in its grain orientation, presence of non-metallic inclusions, galvanic coupling between the composite and the Al substrate, presence of flaws, localized deterioration and heterogeneous surface properties [12–16]. Generally, AMMC materials are more vulnerable to corrosion damage compared to monolithic Al despite improved mechanical properties. However, knowledge of the corrosion resistance behaviour of AMMC analogous to alumina weight composition and grain size will aid proper material selection for application in corrosive industrial environments. This study targets the influence of limited alumina grain size and concentration on the corrosion resistance of AA1070 aluminium.

2. Experimental methods

AA1070 monolithic aluminium alloy (AA1070) acquired from Aluminium Rolling Mills Company, Ota, Ogun State, Nigeria possesses ostensible (wt. %) constituent presented in Table 1. Alumina nano-grains (Al_2O_3) of 150 nm and 600 nm were acquired from the Department of Civil Engineering, Covenant University, Ota, Ogun State, Nigeria. The grains were incorporated into smelted AA1070 at 650 °C through stir cast method to obtain Al alumina matrix composites (AA1070/Al_2O_3) at 5% and 10% weight composition for 150 nm and 600 nm alumina grain sizes as shown in Table 2. The smelted AA1070/Al_2O_3 was mixed through an automated mechanism, ejected into sand molds and cooled for 24 h. AA1070 and AA1070/Al_2O_3 were cut to achieve regular surface area of 1 cm^2. The samples underwent metallographic preparation (after embedding in acrylic mounts) with emery papers of 60, 120, 220, 600, 800 1000 grits and diamond polishing fluid (6 μm), prior to washing with deionized H_2O and propanone for potentiodynamic polarization and open circuit potential analysis. The Brinell hardness, conductivity and ultimate tensile strength data are laid out in Table 3. 0.0125 M H_2SO_4 solution was prepared from standard grade H_2SO_4 acid (98%, acquired from Sigma Aldrich) with deionized H_2O. Standard grade NaCl acquired from Loba Chemie PVT. Ltd., Mumbai, India was prepared in cubic concentration of 3.5% NaCl in deionized H_2O, while 0.0125 M H_2SO_4/3.5% NaCl was prepared from standard grade H_2SO_4 acid and NaCl. Potentiodynamic polarization plots were obtained at sweep rate of 0.0015 V/s between −1.65 V and +0.35 V. The potential was stabilized for 10 min before polarization to attain quasi-steady state. Corrosion current density (A/cm^2) and corrosion potential (V) values were obtained from Tafel extrapolation of anodic–cathodic polarization plots. Corrosion rate C_R (mm/y) was computed from the mathematical equation below (Eq. (1));

$$C_R = 0.00327 \times C_D \times E_Q / D \quad (1)$$

Table 2
Description of AA1070 and AA1070/alumina samples.

Sample	Weight fraction of Alumina (wt. %)	Particle size of alumina	Weight fraction of Al matric (wt.%)
A	–	–	100
B1	5	150 nm	95
B2	5	600 nm	95
B3	10	150 nm	90
B4	10	600 nm	90

Table 3
Brinell hardness, conductivity and ultimate tensile strength data for AA1070 and AA1070/alumina samples at 150 and 600 nm grain sizes.

Sample	Hardness (HBS)	Conductivity (MΩ/m)	
A	12.7	94.88	52.99
B1	13.73	36	119.76
B2	12.95	33.77	119.76
B3	14.9	33.48	124.41
B4	14.59	32.78	121.5

E_Q represents equivalent weight (g) of the AA1070 alloys, 0.00327 indicates corrosion rate constant for dimension and time conversion in mm/y and D represents density (g). The potentiostatic instrument was examined for any conceivable cause of systematic errors. The uncertainty of single measurement is limited by the precision and accuracy of the measuring instrument. As a result, calibration of the instrument and hardware test was performed with the results shown in Table 4. Test for reproducibility of consistent results was also performed and proven to be okay. Open circuit potential analysis on AA1070 and AA1070/Al_2O_3 placed within 200 ml of 3.5% NaCl, 0.0125 M H_2SO_4 and 0.0125 M H_2SO_4/3.5% NaCl solution was done at step potential of 0.1 V/s for 2700 s with 2 electrode configuration (Ag/AgCl reference electrode and vercocit mounted aluminium alloy electrode) coupled to Digi-Ivy 2311 potentiostat.

3. Results and discussion

3.1. Potentiodynamic polarization studies

Potentiodynamic polarization plots of AA1070 (A) and AA1070 at specific alumina composition and grain size (B1, B2, B3 and B4) corrosion in 0.0125 M H_2SO_4, 3.5% NaCl, and 0.0125 M H_2SO_4-3.5% NaCl solutions are shown in Fig. 1(a), (b) and (c). The potentiodynamic polarization data obtained is shown in Table 5. Inspection of Table 5 shows the corrosion rate of AA1070 samples from 0.0125 M H_2SO_4-3.5% NaCl solution exhibited the highest corrosion rate results compared to the corrosion rate values obtained in 0.0125 M H_2SO_4 and 3.5% NaCl solutions. This is due to the combined electrochemical action of SO_4^{2-} and Cl^- which rapidly destroyed the protective oxide on the composite alloy. The oxide becomes unstable and deteriorates locally leading to localized corrosion [17,18]. Sample A exhibited corrosion rate of 5.933 mm/y analogous to corrosion current density of 5.47×10^{-4} A/cm^2 and polarization resistance of 46.98 Ω. Addition of alumina composite to sample A at 5% wt. composition and 150 nm grain size (sample B1) results in increase in corrosion rate to 6.682 mm/y due to two reasons (1) discontinuities in its grain orientation and heteroge-

Table 1
Nominal constituent of AA1070.

Element Identification	Fe	Si	Mn	Cu	Mg	Ti	Al
% Constituent	0.25	0.2	0.03	0.04	0.03	0.05	99.33

Table 4
Results of calibration and hardware test.

RAM Test	
Ok	
Current Test Results	
Sensitivity offset error (0%)	Gain error (0%)
Voltage Test Results	
Sensitivity offset error (0%)	Gain error (0%)

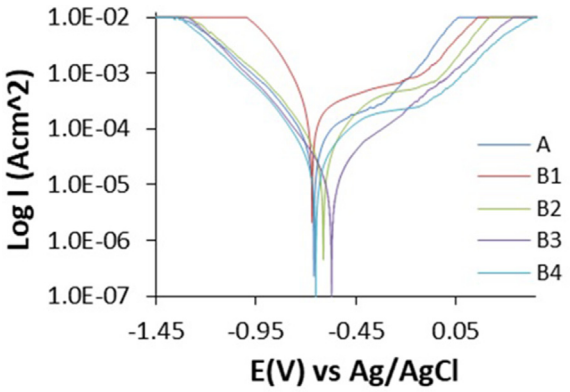

Fig. 1. Potentiodynamic polarization plots output for AA1070 and AA1070 at specific aloxide wt.% composition and grain size in (a) 0.0125 M H_2SO_4, (b) 3.5% NaCl and (c) 0.0125 M H_2SO_4-3.5% NaCl.

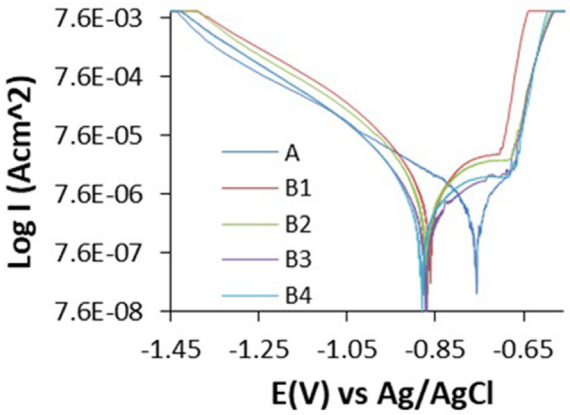

Fig. 1 (*continued*)

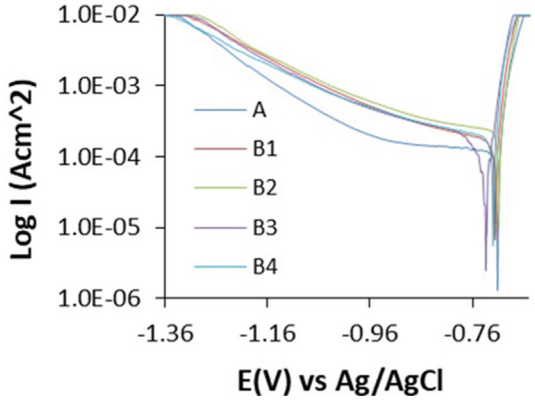

Fig. 1 (*continued*)

neous surface properties of the matrix composite and (2) insufficient or non-resilient Al_2O_3 oxide layer on the composite [19]. Decrease in corrosion rate occurred after sample B1 (i.e. sample B2 – B4) analogous to variation in alumina composition and grain size due to build-up of sufficient oxide layer/thickness and its ability to impart sufficient passivity on AA1070. The polarization plot in Fig. 1(c) shows extensive cathodic reaction behaviour resulting from H_2 evolution and O_2 reduction reaction mechanism precipitated by action of SO_4^{2-} and Cl^- anions. The anions react on the matrix surface, and cathodic reactions from adjacent precipitates occurs on the matrix surface. Galvanic interactions between the matrix, precipitates and intermetallic phases on the composite results in heterogeneous reaction mechanisms whereby adjacent sites tends to be cathodic to the bulk alloy substrate [20]. Anodic polarization plots associated with surface degradation exhibits very high slopes and appear to be under activation control mechanism, thus indicating rapid acidification of the composite surface; though this is probable for the cathodic reaction plots from sample B1 to B4 [21]. Nevertheless, this affirmation is confirmed from the near similarities of the anodic–cathodic Tafel slope values in Table 5.

The plot configuration in Fig. 1(a) and (b) significantly differ from each other due to differences in the surface reaction mechanism on sample A to B4 resulting from the action of SO_4^{2-} in H_2SO_4 solution and Cl^- in NaCl solution. The high reactivity and size of Cl^- enhance the localized deterioration on the matrix samples resulting in miniature current transient on the anodic plot in Fig. 1(b) [22,23]. However, significant passivation behaviour was observed before instantaneous transition to stable pitting. This occurred due to breakdown of the passive film induced by alumina composite [24,25]. The corrosion rate results increase in value from sample A to B1 (0.062–0.084 mm/y) similar to the observation in 0.0125 M H_2SO_4-3.5% NaCl solutions. Beyond sample B1, substantial reduction in corrosion rate occurred analogous to alumina wt. % composition and grain size to 0.031 mm/y for sample B4. The corrosion rate value is representative of general surface deterioration. However, the anodic slope configuration shows sample B1 and B2 exhibits relatively weak resistance to anodic dissolution and pitting corrosion which is a major destructive mechanism on composites [26]. Decrease in corrosion potential data from −0.756 V to −0.879 V in Table 4 from sample A to B4 confirms the effect of localized deterioration on the matrix samples. This variation is also associated with cathodic reaction mechanism which tends to occur between the precipitates within the matrix metallurgical structure [27]. The effect of SO_4^{2-} anions on the matrix composites is evident in Fig. 1(a). The reaction mechanism of SO_4^{2-} tends to occur generally over the entire surface of the samples compared to Cl^- anion. Hence its cathodic polarization slopes for samples A, B2, B3 and B4 are generally the same due to activation control mechanism. However, the anodic polarization plots vary substantially due to significant anodic degradation mechanism on the matrix samples. This is shown in the anodic Tafel slope values in Table 5 due to higher anodic exchange current density [28]. Sample B1 exhibited the highest slope configuration signifying high deterioration reaction which is proven from its corrosion rate output of 0.684 mm/y. Limited passivation behaviour occurred on the anodic polarization plots. Comparing the corrosion rate results from H_2SO_4 solutions to the other electrolyte solutions, it is evident that the matrix composites in NaCl solution exhibited the lowest corrosion rate values while the combined H_2SO_4 and NaCl solution induced the highest corrosion rate values. The reason for B4 having the lowest corrosion rate in all the electrolytes studied is because the protective film/oxide formed on composite is Al_2O_3 i.e. alumina and it tends to be more resilient compared to other composite specimens. Secondly, aluminium composite exhibits a heterogonous microstructure leading to discontinuous film on the composite surface.

Table 5
Potentiodynamic polarization output for AA1070 and AA1070 at specific alumina wt.% composition and grain size.

0.0125 M H_2SO_4							
Alumina Composition (%)	**Corrosion Rate (mm/y)**	**Corrosion Current (A)**	**Corrosion Current Density (A/cm^2)**	**Corrosion Potential (V)**	**Polarization Resistance, R_p (Ω)**	**Cathodic Tafel Slope, B_c (V/dec)**	**Anodic Tafel Slope, B_a (V/dec)**
A	0.346	3.19 E−05	3.19 E−05	−0.661	805.70	−7.014	5.051
B1	0.684	6.31E−05	6.31 E−05	−0.670	197.00	−8.501	3.495
B2	0.234	2.16 E−05	2.16 E−05	−0.613	1191.00	−7.165	6.733
B3	0.149	1.37 E−05	1.37 E−05	−0.572	3069.00	−7.761	4.255
B4	0.117	1.08 E−05	1.08 E−05	−0.651	1740.00	−7.254	5.843
3.5% NaCl							
Alumina Composition (%)	**Corrosion Rate (mm/y)**	**Corrosion Current (A)**	**Corrosion Current Density (A/cm^2)**	**Corrosion Potential (V)**	**Polarization Resistance, R_p (Ω)**	**Cathodic Tafel Slope, B_c (V/dec)**	**Anodic Tafel Slope, B_a (V/dec)**
A	0.062	5.75 E−06	5.75 E−06	−0.756	4472.00	−6.330	5.450
B1	0.084	7.73 E−06	7.73 E−06	−0.860	3323.00	−9.986	5.559
B2	0.035	5.65 E−06	3.25 E−06	−0.866	4551.00	−10.040	5.396
B3	0.034	3.10 E−06	3.10 E−06	−0.868	8277.00	−10.400	6.009
B4	0.031	2.85 E−06	2.85 E−06	−0.879	9037.00	−14.600	5.781
0.0125 M H_2SO_4-3.5% NaCl							
Aloxide Composition (%)	**Corrosion Rate (mm/y)**	**Corrosion Current (A)**	**Corrosion Current Density (A/cm^2)**	**Corrosion Potential (V)**	**Polarization Resistance, R_p (Ω)**	**Cathodic Tafel Slope, B_c (V/dec)**	**Anodic Tafel Slope, B_a (V/dec)**
A	5.933	5.47 E−04	5.47 E−04	−0.711	46.98	−0.271	4.062
B1	6.682	6.16 E−04	6.16 E−04	−0.716	41.80	−1.598	4.183
B2	4.992	4.60 E−04	4.60 E−04	−0.709	29.87	−1.057	4.016
B3	3.827	3.53 E−04	3.53 E−04	−0.734	101.70	−1.899	4.167
B4	2.192	2.02 E−04	2.02 E−04	−0.720	36.60	−1.187	4.073

Addition of alumina increases the volume fraction of the protective oxide on the aluminium composite leading to thicker and continuous protective oxide on the surface. This invariably increases corrosion rate of the matrix composite.

3.2. Open circuit potential analysis

The corrosion potential plots for AA1070 and AA1070 at specific alumina wt. % composition and grain size (sample A, B1 and B4) from 0.0125 M H_2SO_4, 3.5% NaCl and 0.0125 M H_2SO_4-3.5% NaCl solutions are presented from Fig. 2(a) to (c). Inspection of the plots in the figures shows the plots configurations in Fig. 2(a) is relatively the most electropositive compared to the plots in Fig. 2(b) and (c). This is due to the distinct electrochemical action of SO_4^{2-} anions compared to Cl^- and SO_4^{2-}/Cl^-. The large size of SO_4^{2-} anions hinders its localized corrosion reaction mechanism [29,30]. Its actions tend to be general surface deterioration. Sample B4 [Fig. 2(a)] exhibited the lowest tendency to corrode with corrosion potential value culminating at −0.595 V (2700 s). This observation

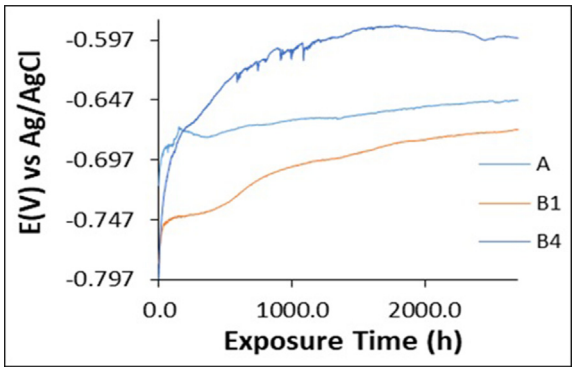

Fig. 2. OCP plots for AA1070 and AA1070 at specific alumina wt. % composition and grain size in (a) 0.0125 M H_2SO_4, (b) 3.5% NaCl and (c) 0.0125 M H_2SO_4-3.5% NaCl.

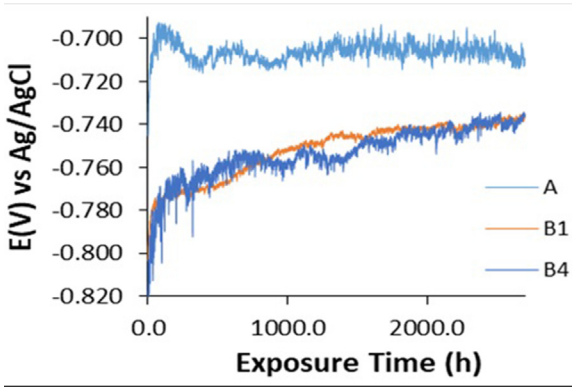

Fig. 2 (*continued*)

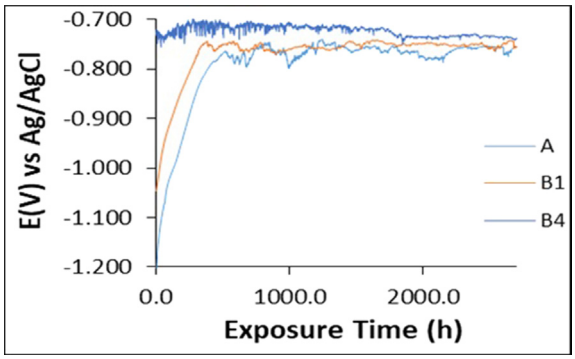

Fig. 2 (*continued*)

agrees with the data from potentiodynamic polarization which shows sample B4 had the lowest corrosion rate with sample B1 being the most electronegative on Fig. 1(a). The plots show a pro-

gressive shift to electropositive values and the distinct absence of major potential transients [31]. Hence, despite the higher corrosion rate of samples A, B1 and B4 in H_2SO_4 compared to NaCl solution, the matrix samples are thermodynamically stable in H_2SO_4 solution. Comparing Fig. 2(b) to 2(c), observation shows the potential transients in Fig. 2(c) are significantly higher than the observation in Fig. 2(b) due to the admixed electrochemical action of SO_4^{2-} and Cl^- anions compared to Cl^- anion only in Fig. 2(b) [32,33]. The potential transients are due to thermodynamic instability of the passive film on the matrix samples resulting in active–passive transition behaviour during potential scanning [34]. The large potential transient exposes the matrix composites to corrosion reaction mechanism resulting in surface deterioration of the composite; hence the relatively high corrosion rate result from 0.0125 M H_2SO_4-3.5% NaCl solutions compared to the others. The transients occurred through the exposure time. However, the plot configuration in Fig. 2(c) for sample A and B1 progressed steeply to relative electropositive values due to build-up of the passive oxide on the composites before miniature active–passive transition behaviour. The low potential transient shows the matrix composite surface is partly resistance to corrosion though thermodynamically unstable. However, the plot configuration for sample B4 displayed extensive potential transient which decreased with respect to exposure time. Observation of all the plots shows the matrix composites is more thermodynamically stable in H_2SO_4 solution which low tendency to corrode despite the contrary from potentiodynamic polarization studies. Whereas the plot configuration from NaCl solution shows thermodynamic imbalance, but surface resistance to corrosion at higher corrosion tendencies while the plots in Fig. 2(c) exhibited the highest tendency to corrode.

4. Conclusion

AA1070 aluminium alloy reinforced with alumina material at 5% weight composition and 150 nm nano grain sizes exhibited the highest vulnerability to corrosion in H_2SO_4, NaCl and combined H_2SO_4 and NaCl solutions compared to monolithic AA1070 aluminium alloy and aluminium alloy at specific weight compositions and nano grain sizes studied. At 10% alumina weight composition, and 150 nm and 600 nm nano grain size progressive decrease in corrosion rate occurred below the value obtained for the monolithic aluminium alloy due to enhanced protective oxide on the monolithic aluminium alloy. The combined H_2SO_4 and NaCl solutions was proven to be the most deleterious environment studied due to the relatively higher corrosion rates obtained compared to the values obtained from H_2SO_4 and NaCl solution individually. Corrosion potential plots from open circuit potential analysis shows lower tendency to corrode and higher thermodynamic stability in H_2SO_4 solution for the monolithic and alumina reinforced aluminium alloy. In the combined H_2SO_4-NaCl solution significant potential transients were visible signifying chaotic thermodynamic behaviour and increased tendency to corrode which is in agreement with the results from potentiodynamic polarization studies.

CRediT authorship contribution statement

Roland Tolulope Loto: Supervision, Conceptualization, Writing – original draft, Visualization, Investigation, Validation, Data curation. **Philip Babalola:** Supervision, Conceptualization, Writing – original draft, Visualization, Investigation, Validation, Data curation.

Declaration of Competing Interest

The authors declare that they have no known competing financial interests or personal relationships that could have appeared to influence the work reported in this paper.

Acknowledgements

The author is grateful to Covenant University Ota, Ogun State, Nigeria for their support for this project.

References

[1] R.T. Loto, P. Babalola, J. Sánchez, Corrosion polarization behavior and microstructural analysis of AA1070 aluminium silicon carbide matrix composites in acid chloride concentrations, Cogent Eng. 4 (1) (2017) 1422229, https://doi.org/10.1080/23311916.2017.1422229.
[2] C.A Loto, O.O Joseph, R.T Loto, Adsorption and inhibitive properties of Camellia Sinensis for aluminium alloy in HCl, Int. J. Elect. Sci. 9 (7) (2014) 3637–3649. http://www.electrochemsci.org/papers/vol9/90703637.pdf, In this issue.
[3] G.S. Cole, A.M. Sherman, Lightweight materials for automotive applications, Mater. Charact. 35 (1) (1995) 3–9.
[4] W.S. Miller, L. Zhuanga, J. Bottemaa, A.J. Wittebrood, P. De Smet, A. Haszlerc, A. Vieregge, Recent development in aluminium alloys for the automotive industry, Mater. Sci. Eng. A 280 (1) (2000) 37–49.
[5] P. Garg, A. Jamwal, D. Kumar, K.K. Sadasivuni, C.M. Mustansar Hussain, P. Gupta, Advance research progresses in aluminium matrix composites: manufacturing & applications, J. Mater. Res. Technol. 8 (5) (2019) 4924–4939.
[6] A.J. Ruys, Alumina Ceramics: Biomedical and Clinical Applications, Woodhead Publishing, UK, 2018.
[7] M. Schacht, N. Boukis, E. Dinjus, Corrosion of alumina ceramics in acidic aqueous solutions at high temperatures and pressures, J. Mater. Sci. 35 (24) (2000) 6251–6258, https://doi.org/10.1023/A:1026714218.
[8] L. Ćurković, M.F. Jelača, S. Kurajica, Corrosion behavior of alumina ceramics in aqueous HCl and H_2SO_4 solutions, Corros. Sci. 50 (3) (2008) 872–878.
[9] K.R. Mikeska, S.J. Bennison, Corrosion of alumina in aqueous hydrofluoric acid, J. Am. Ceram. Soc. 82 (12) (1999) 3561–3566.
[10] R.T. Loto, A. Adeleke, Corrosion of aluminum alloy metal matrix composites in neutral chloride solutions, J. Fail. Anal. Prev. 16 (5) (2016) 874–8851.
[11] R.T. Loto, Phillip Babalola, Electrochemical analysis of SiC composite additions at 7.5% weight content on the corrosion resistance of monolithic aluminium alloy in sulphate–chloride solution, J. Mater. Res. Technol. 8 (3) (2019) 2517–2527.
[12] R.T. Loto, Investigation of the localized corrosion resistance of 4044 aluminum alloy in acid chloride and neutral chloride solutions, J. Fail. Anal. Preven. 18 (2018) 905–911.
[13] K. Alaneme, M. Bodunrin, Corrosion behavior of alumina reinforced aluminium (6063) metal matrix composites, J. Miner. Met. Mater. Eng. 10 (12) (2011) 1153–1165, https://doi.org/10.4236/jmmce.2011.1012088.
[14] D.M. Aylor, D. Taylor, Corrosion of Metal Matrix Composites, ASM Handbook, OH, 1999, pp. 859–863.
[15] M. Rahimian, N. Parvin, N. Ehsani, The effect of production parameters on microstructure and wear resistance of powder metallurgy Al-Al_2O_3 composite, Mater. Des. 32 (2011) 1031–1038, https://doi.org/10.1016/j.matdes.2010.07.016.
[16] M. Kok, K. Ozdin, Wear resistance of aluminum alloy and its composites reinforced by Al_2O_3 particles, J. Mater. Process Technol. 183 (2–3) (2007) 301–309, https://doi.org/10.1016/j.jmatprotec.2006.10.021.
[17] P. Schmuki, From Bacon to barriers: a review on the passivity of metals and alloys, J. Solid State Electrochem. 6 (2002) 145–164.
[18] C.L. Chang, M.H. Engelhard, S. Ramanathan, Superior nanoscale passive oxide layers synthesized under photon irradiation for environmental protection Appl, Phys. Lett. 92 (2008) 263103.
[19] P.M. Natishan, W.E. O'Grady, Chloride ion interactions with oxide-covered aluminum leading to pitting corrosion: a review, J. Electrochem. Soc. 161 (9) (2014) C421–C432.
[20] Yakun Zhu, Kai Sun, G.S. Frankel, Intermetallic phases in aluminum alloys and their roles in localized corrosion, J. Electrochem. Soc. 165 (11) (2018) C807–C820.
[21] Y. Cao, C. Zou, C. Wang, H. Liang, W. Chen, W. Li, Effect of TiO2 nanoparticles and SDBS on corrosion behavior of 3003 aluminum alloy in aqueous ethylene glycol containing chloride ions at high temperature, J. Alloy Compd. 873 (2021) 159820.
[22] C. Vargel, Corrosion of Aluminium, second ed., 2020.
[23] Y. Song, G. Jiang, Y. Chen, P. Zhao, Y. Tian, Effects of chloride ions on corrosion of ductile iron and carbon steel in soil environments, Sci. Rep. 7 (2017) 6865.
[24] Hemalatha Parangusan, Jolly Bhadra, Noora Al-Thani, A review of passivity breakdown on metal surfaces: influence of chloride- and sulfide-ion concentrations, temperature, and pH, Emergent Mater. 4 (5) (2021) 1187–1203, https://doi.org/10.1007/s42247-021-00194-6.

[25] H. Parangusan, J. Bhadra, N. Al-Thani, A review of passivity breakdown on metal surfaces: influence of chloride- and sulfide-ion concentrations, temperature, and pH, Emergent Mater. 4 (2021) 1187–1203.
[26] G.R. Kramera, C.M. Méndeza, A.E. Ares, Evaluation of corrosion resistance of commercial aluminum alloys in ethanol solutions, Mater. Res. 21 (6) (2018) e20170272.
[27] M. Gobara, A. Barakaa, R. Akidb, M. Zorainy, Corrosion protection mechanism of Ce4+/organic inhibitor for AA2024 in 3.5% NaCl, RSC Adv. 10 (2020) 2227–2240.
[28] A.K. Vijh, Electrolytic hydrogen evolution reaction on aluminum, oxide-covered electrodes, Phys. Chem. 73 (3) (1969) 506–513.
[29] L. Yang, Y. Xu, Y. Zhu, L. Liu, X. Wang, Y. Huang: Evaluation of interaction effect of sulfate and chloride ions on reinforcements in simulated marine environment using electrochemical methods, Int. J. Electrochem. Sci., 11 (2016) 6943–6958 http://doi.org/10.20964/2016.08.51.
[30] W. JinLee, S. IlPyun, Effects of sulphate ion additives on the pitting corrosion of pure aluminium in 0.01 M NaCl solution, Electrochim. Acta 45 (12) (2000) 1901–1910.
[31] A.C. Bastos, M.G.S. Ferreira, Application of the scanning vibrating electrode technique to the characterization of modern coatings, in: Handbook of Modern Coating Technologies, 2021, pp. 1–43.
[32] C. Christodoulou, C.I. Goodier, S.A. Austin, J. Webb, G. Glass, On-site transient analysis for the corrosion assessment of reinforced concrete, Corros. Sci. 62 (2012) 176–183.
[33] Hugh S. Isaacs, Yuichi Ishikawa, Current and potential transients during localized corrosion of stainless steel, J. Electrochem. Soc. 132 (6) (1985) 1288–1293.
[34] R. Ramanathan, P.W. Voorhees, Morphological stability of steady-state passive oxide films, Electrochim. Acta 303 (2019) 299–315.